Doctor of Philosophy

# DRG2 depletion induces Golgi fragmentation via GSK3β phosphorylation and microtubule stabilization

The Graduate School

Of the University of Ulsan

Department of Biological Science

Kim, Beom-Chang

# DRG2 depletion induces Golgi fragmentation via GSK3β phosphorylation and microtubule stabilization

Supervisor : Park, Jeong-Woo

A Dissertation

Submitted to
The Graduate School of the University of Ulsan
In partial Fulfillment of the Requirements
for the Degree of

Doctor of Philosophy

By

Kim, Beom-Chang

Department of Biological Science
Ulsan, Korea

June, 2020

**DRG2 depletion induces Golgi fragmentation via GSK3β phosphorylation and microtubule stabilization**

This certifies that the dissertation thesis

of Kim, Beom-Chang is approved

Committee Chair Prof. Lee, Byung-Ju

Committee Prof. Park, Jeong-Woo

Committee Prof. Jeong, Choon Soo

Committee Prof. Chung, Hun-Taeg

Committee Prof. So, Hong-Seob

Ulsan, Korea

June, 2020

**CONTENTS**

## Abstract

The perinuclear stacks of the Golgi apparatus maintained by dynamic microtubules are essential for cell migration. Here, we show that DRG2 plays a key role in regulating microtubule stability, perinuclear Golgi stack formation, and cell migration. DRG2 depletion prolonged the EGFR localization in endosome, enhanced Akt activity and inhibitory phosphorylation of GSK3β. Tau, a target of GSK3β, was hypo-phosphorylated in DRG2-depleted cells and showed greater association with microtubules, resulting in microtubule stabilization. Stabilized microtubules were resistant to depolymerization by nocodazole. DRG2-depleted cells showed defects in microtubule growth and microtubule organizing centers (MTOC), Golgi fragmentation, and loss of directional cell migration. These results reveal a previously unappreciated role for DRG2 in the regulation of perinuclear Golgi stacking and cell migration via its effects on GSK3β phosphorylation, and microtubule stability.

**Key words**: DRG2, GSK3β, microtubule stability, Golgi fragmentation, cell migration

## Introduction

The Golgi apparatus is a perinuclear membranous organelle that mediates protein and lipid transport and modification. Formation of stable multilayer stacks is essential for proper Golgi functioning (1, 2). Golgi defects affect protein trafficking, sorting, and modification, and Golgi fragmentation has been observed in viral infections and in diseases such as cancer and neurodegeneration (3, 4). Formation of the Golgi ribbon relies on a microtubule cytoskeleton emanating from microtubule organization centers (MTOCs) (5, 6). The Golgi matrix protein GMAP210 binds γ-tubulin in the MTOC (7, 8), and the peripheral Golgi protein golgin-160 interacts with the dynein-dynactin microtubule motor complex, leading to concentration of Golgi stacks in the pericentriolar region (9, 10).

Microtubules dynamically switch between growing and shrinking phases at their ends (11). The importance of microtubule dynamics in Golgi stack formation is highlighted by the finding that both microtubule stabilizing and destabilizing drugs disrupt the Golgi complex. Nocodazole-induced microtubule depolymerization causes Golgi fragmentation (12, 13). After drug removal, Golgi elements translocate along newly repolymerized microtubules to reassemble an intact Golgi complex (13). Hyper-stabilization of microtubules by taxol also induces Golgi fragmentation. Taxol treatment causes accumulation of microtubule bundles in the cell periphery (14, 15) and loss of a unified perinuclear structure near the MTOC, resulting in Golgi fragmentation (16).

Tau is a microtubule-associated protein that interacts with α- and β-tubulin and stabilizes microtubules in both neuronal (17) and non-neuronal cells (18). This process is regulated by the phosphorylation of Tau at serine and threonine residues (19). Several kinases and phosphatases are involved in regulation of Tau phosphorylation, including glycogen synthase kinase 3β (GSK3β) (20).

GSK3β activity is controlled by endosomal signaling. Endocytosis of cell surface receptors is stimulated by ligand-induced activation and activated receptors in endosomes can continue to transmit signals that are different from those that arise from the plasma membrane (21). Endosomes containing EGFR together with the GTPase Rab5 and its effectors, APPL1 and APPL2, can serve as specialized signaling endosomes (22). APPLs recruited to the endosomal membrane by Rab5 activate Akt (23), resulting in inhibitory phosphorylation of GSK3β on Ser-9 (24). In a similar example of endosome signaling, Rab5 has been shown to participate in the endocytosis of insulin receptors (25), resulting in increased Akt phosphorylation and reduced GSK3 activity (26). Depletion of Rab5 reduced the insulin-stimulated phosphorylation of Akt (27).

Developmentally regulated GTP-binding proteins (DRGs) are a novel class of GTPase (28) consisting of two closely related proteins, DRG1 and DRG2 (29). Previously, we found that cell lacking DRG2 showed defects in endosomal Rab5 deactivation and EGFR accumulation (30) suggesting that loss of DRG2 enhances Akt activity and inhibitory GSK3β phosphorylation in endosomes. Here, we demonstrate that DRG2 depletion dramatically increases Akt activity and inhibitory phosphorylation of GSK3β, which results in reduced phosphorylation of Tau, extremely stable microtubule structures and Golgi fragmentation. Furthermore, cells lacking DRG2 show loss of directional cell migration. These results provide the first demonstration of the functional significance of DRG2 in microtubule dynamics, Golgi stacking, and cell migration. DRG2 expression may represent a novel therapeutic target for treating and preventing diseases caused by defects in microtubule dynamics and Golgi structure.

## Materials and Methods

### Cell culture

Wild-type and DRG2-depleted mouse embryonic fibroblasts and DRG2-stably depleted HeLa cells (30) were maintained in DMEM supplemented with 10% FBS (Invitrogen). LY294002 (BIOMOL) at 100 nM was used to inhibit PI3K activity. LiCl (Sigma-Aldrich) at 1 mM was used to inhibit GSK3β. Dynasore (Sigma-Aldrich) at 80 μM was used to inhibit dynamin. Nocodazole (Sigma-Aldrich) at 1 μM was used to disrupt microtubule function.

### Plasmids, shRNAs, and transfections

An shRNA-resistant p3XFLAG hDRG2 construct (p3XFLAG.hDRG2) was described previously (31). The following plasmid constructs were purchased from Addgene: pIRESneo-EGFP-α-tubulin (Patricia Wadsworth, University of Massachusetts, USA), mEmerald-Golgi-7 (beta-1,4-galactosyltransferase 1), tdTomato-Golgi-7 (beta-1,4-galactosyltransferase 1) (Michael Davidson, Florida State University, USA), pEB1-2xEGFP (Torsten Wittmann, University of California, San Francisco, USA), pAdEasy-mRFP-GSK3β S9A (Torten Wittmann, University of California, San Francisco, USA), VSV-G-GFP (*ts*O45) VSVG-GFP (ts045 VSVG tagged with green fluorescent protein) (Jennifer Lippincott-Schwartz, NIH, USA), WT dynamin 1 pEGFP , K44A dynamin 1 mRFP (Sandra Schmid, UT Southwestern Medical Center, USA), and pcDNA3-AktAR2 (Jin Zhang, University of California, San Diego, USA).

Cells were transfected with plasmid constructs using TurboFect (Thermo Scientific). To monitor transfection efficiency, the GFP expression vector pEGFP-N1/C1 (Clontech) was cotransfected with the plasmid construct. After confirming transfection efficiency to be >80%,

cells were used for further study.

**SDS-PAGE and immunoblotting**

Proteins in cell lysates were resolved by SDS-PAGE, transferred onto nitrocellulose membranes (Amersham Biosciences, Inc.), and probed with appropriate dilutions of the following antibodies: anti-human DRG2, anti-phospho-GSK3β (Y216), and anti-β-actin (Sigma); anti-Akt, anti-phospho-Akt (S473), anti-GSK3β, anti-phospho-GSK3β (S9), anti-acetyl-α-tubulin, anti-Tau, and anti-phospho-Tau (Cell Signaling Technology); and anti-α-tubulin (Santa Cruz Biotechnology and Clontech). Immunoreactivity was detected using a GE HealthCare Image Quant system.

**VSV-G transport**

Cells were transiently cotransfected with constructs encoding VSV-G-ts045–GFP and tdTomato-Golgi-7 and incubated for 16 h at 40.5℃. Cells were further incubated for 30 min with 100 μM cycloheximide and shifted to 32℃ to release the VSV-G proteins from the ER. After incubation for an indicated time period at 32℃, cells were subsequently fixed 3.7% paraformaldehyde and processed for confocal microscopy with 1200 laser scanning confocal system (Olympus). Colocalization of VSV-G with Golgi was quantified using the "colocalization analysis" plugin of the NIH ImageJ software.

**Confocal microscopy**

Cells on glass coverslips were transfected with various plasmid constructs for 24 h. Cells were washed twice with DMEM-HEPES (without phenol-red, with 25 mM HEPES; GIBCO) and incubated for 12 h with serum-free media. Cell were then incubated in DMEM-HEPES

containing 100 ng/ml EGF for the indicated times. Cells were washed 3x with ice-cold PBS and fixed with 3.7% paraformaldehyde (Sigma) in PBS. After cell permeabilization with 0.2% Triton X-100 in PBS and blocking with blocking solution (10 mM Tris-Cl pH 7.4, 100 mM MgCl2, 0.5% Tween 20, 3% BSA, 5% FBS), endogenous α-tubulin, acetylated α-tubulin, phospho-Akt, and Tau were stained using antibodies described above.

Confocal images were acquired in sequential mode using the appropriate filter combination on an Olympus FV1200 laser-scanning confocal system or a Zeiss LSM 700/780 at the Ulsan National Institute of Science and Technology (UNIST) Bio-imaging Center. To minimize artifacts caused by overexpression of genes, images were collected from cells with moderate expression levels. All images were saved as TIFF files, and their contrast was adjusted using Image J. Pixel-by-pixel colocalization analysis was performed using ImageJ (JACoP plug-in) (32). Images were analyzed using MetaMorph 7 software (Universal Imaging, West Chester, PA) and Imaris Bitplane-7.7.2 at the UNIST Bio-imaging Center. Live cell images were acquired at 37℃ every min. Videos were generated with Image J.

**Measurement of microtubule nucleation and growth using EB1-GFP**

Cells on glass coverslips coated with poly-D-lysine (Neuvitro) were transfected with pEB1-2xEGFP. Images were acquired every 0.1 s for a total of 1 min for each time-lapse movie. The number of EB1-GFP growth events and microtubule growth rates were obtained by tracking EB1-GFP comets at microtubule plus-ends using PlusTipTracker software (33).

**FRET analysis of Akt activity**

Akt activity reporter (pcDNA3-AktAR2) was used as a FRET probe to analyze Akt activity *in vivo*. AktAR consists of Cerulean3 (a brighter variant of CFP), the forkhead-associated

domain (FHA1) (used as the phosphoamino acid binding domain), the Akt substrate sequence (derived from the sequence surrounding Thr24 of FOXO1), and cpV E172 (a brighter variant of Venus) (34, 35). FRET analysis for Akt activity was conducted as described previously (34, 35). Briefly, control and DRG2-depleted cells were transfected with pcDNA3-AktAR2 and serum starved for 12 h. Images were acquired on the Olympus FV1200 system with a cooled high-sensitivity detector. Dual-emission ratio imaging was performed using a 420DF20 excitation filter, 450DRLP dichroic mirror, and two emission filters, 475DF40 and 535DF25, for CFP and YFP, respectively. Images were processed with ImageJ and Metamorph software. After background subtraction, FRET ratio images were generated using MetaMorph and visualized in intensity-modulated display mode. In this display mode, eight colors from red to blue are used to represent the FRET ratio (YFP/CFP), with the intensity of each color indicating the mean intensity of YFP and CFP.

**Statistical analysis**

Unpaired Student's *t*-tests (two-tailed) were used to determine the significance of differences between groups. *P* values $<0.05$ were considered significant.

## RESULTS

### Golgi fragmentation in DRG2-depleted cells

Vesicular stomatitis virus glycoprotein (VSV-G) ts045, a temperature-sensitive variant of VSV-G, resides in the ER at 40.5℃ but moves into the Golgi complex upon temperature reduction to 32℃ (36, 37). To determine whether DRG2 affects trafficking of cargo from ER to Golgi, DRG2-depleted and control HeLa cells (Fig. 1A) were transfected with VSV-G ts045-GFP, incubated at 40.5 ℃ for 16 h, then shifted to 32℃, and monitored for trafficking of VSV-G. Within 15 min of shifting to 32℃, the VSV-G in control cells accumulated at the perinuclear region (Fig. 1B). However, in DRG2-deleted cells, perinuclear accumulation of VSV-G was not detected until 30 min after the temperature change and VSV-G was present in cytoplasmic scattered structures (Fig. 1B). To confirm the role of DRG2 in VSV-G trafficking, mouse embryonic fibroblast (MEF) cells from wild-type and DRG2-knock out mice (Fig. 1C) were transfected with VSV-G ts045-GFP and monitored for VSV-G trafficking. As in HeLa cells, perinuclear accumulation of VSV-G did not occur until 60 min after shifting to 32℃ in DRG2-depleted MEF cells, whereas it was observed at 15 min after shifting to 32℃ in wild-type MEF cells (Fig. 1D).

To test whether the scattered structures containing VSV-G in DRG2-depleted cells are Golgi, we co-transfected control and DRG2-depleted HeLa cells with VSV-G and a Golgi marker beta-1,4-galactosyltransferase 1 (tdTomato-Golgi-7). At 15 min following temperature shift in DRG2-depleted cells, VSV-G colocalized with Golgi in scattered structures (Fig. 1E). These results demonstrate that DRG2 depletion does not block VSV-G trafficking to Golgi structures, but instead inhibits perinuclear accumulation of Golgi structures containing VSV-G.

We next investigated whether DRG2 depletion affects perinuclear accumulation of Golgi stacks. We assessed Golgi morphology in control and DRG2-depleted HeLa cells stained with anti-GM130 or transfected with tdTomato-Golgi-7. Under confocal microscopy, Golgi structures appeared fragmented and scattered in DRG2-depleted cells and as intact perinuclear Golgi stacks in control cells (Fig. 1F and Supplementary Fig. S1). Approximately 60% of DRG2-depleted cells and <30% of control cells had fragmented Golgi. Next, we tested the effect of ectopic expression of shRNA-resistant DRG2 on Golgi structure in DRG2-depleted cells and found that ectopic DRG2 expression reduced Golgi fragmentation (Fig. 1G). These results demonstrate that DRG2 depletion causes Golgi fragmentation.

**DRG2 depletion inhibits perinuclear MTOC formation and microtubule dynamics**

Formation of perinuclear Golgi stacks relies on an intact microtubule cytoskeleton and MTOC (5, 6). End-binding protein 1 (EB1) is a microtubule plus-end tracking protein that can be used to identify the MTOC. To test whether DRG2 depletion affects perinuclear MTOC formation, we transfected control and DRG2-depleted cells with EB1-GFP and conducted live imaging of the plus ends of microtubules. In control cells, EB1-GFP was initially condensed in a single spot near the nucleus (the MTOC), then moved radially in "comets" toward the plasma membrane (Figs. 2A and 2B; Supplementary Movie 1A). In DRG2-depleted cells, most EB1-GFP comets did not emerge from a single spot and moved in random directions (Figs. 2A and 2B; Supplementary Movie 1B). The rate of nucleation, determined by counting emerging EB1-GFP comets over time (Fig. 2C), and the speed of the GFP-EB1 comets (Fig. 2D) were significantly reduced in DRG2-depleted cells compared with control cells. Ectopic expression of shRNA-resistant DRG2 rescued the radial movement of EB1 from perinuclear MTOCs in DRG2-depleted cells (Fig. 2E).

We also visualized the microtubule networks in control and DRG2-depleted cells by immunofluorescent staining of α-tubulin. In control cells, a region with high microtubule density was detected near the nuclei, and microtubules projected from this region throughout the cytoplasm (Fig. 2F, left); this region was not detected in DRG2-depleted cells (Fig. 2F, middle). Ectopic expression of shRNA-resistant DRG2 in DRG2-depleted cells resulted in a microtubule structure emanating from the perinuclear region (Fig. 2F, right). These data indicate that DRG2 depletion inhibits perinuclear MTOC formation.

Golgi-derived vesicles and Golgi mini-stacks move along microtubules toward the MTOC and are concentrated in the perinuclear region (33). DRG2-related defects in perinuclear MTOC formation and microtubule dynamics led us to test the effect of DRG2 depletion on the movement of Golgi-derived vesicles. To analyze the effect of DRG2 depletion on the repositioning of Golgi during cell migration, we assessed Golgi morphology in control and DRG2-depleted cells stained with anti-α-tubulin and anti-GM130 antibodies or co-transfected with fluorophore-tagged α-tubulin and Golgi-7 which is a Golgi resident enzyme but can translocate to swollen vesicles (39). In control cells, Golgi stacks were concentrated at perinuclear MTOC (Fig. 2G top) and Golgi-derived vesicles moved along the radial array of microtubules to and from the MTOC and were concentrated in the perinuclear region (Fig. 2H left and 2I; Supplementary Movie 2A). In DRG2-depleted cells, perinuclear Golgi stacks were not detected (Fig. 2G bottom) and Golgi-derived vesicles moved more slowly, showed no radial movement, and were dispersed in the cytoplasm (Fig. 2H right and 2I; Supplementary Movie 2B).

**DRG2 depletion enhances microtubule stability**

Microtubule depolymerization by nocodazole leads to Golgi fragmentation (12, 13). We

tested whether DRG2 depletion, which also leads to Golgi fragmentation, affects microtubule stability. As a measure of microtubule stability, we examined the resistance of microtubules to nocodazole. Microtubules in control cells were extensively depolymerized following 60 min of incubation with nocodazole (Fig. 3A). Counter to our expectations, microtubules in DRG2-depleted cells showed slower depolymerization than in control cells, with some microtubules intact after 60 min of incubation with nocodazole (Fig. 3A). We next measured the level of acetylated tubulin, which acumulates in stable microtubules (40). We detected a reduced level of acetylated α-tubulin at 60 min after nocodazole treatment in control cells in immunoblots. In DRG2-depleted cells, the acetylated tubulin level was higher than in control cells even before nocodazole treatment and remained high until 60 min after nocodazole treatment (Fig. 3B). To confirm the role of DRG2 in microtubule stability, DRG2-depleted cells were transfected with shRNA-resistant DRG2 and incubated with nocodazole. Ectopic expression of shRNA-resistant DRG2 in DRG2-depleted cells increased microtubule depolymerization (Fig. 3C) and reduced the level of acetylated α-tubulin (Fig. 3D). These results indicate that DRG2 depletion enhances the stability of microtubule structures.

**DRG2 depletion increases Akt activity and inhibitory phosphorylation of GSK3β**

GSK3β reduces microtubule stability through phosphorylation of Tau, a microtubule-associated protein (41). Phosphorylation of GSK3β at Ser-9 by Akt inhibits GSK3β activity (42). We previously reported that DRG2 depletion enhances endosomal Rab5 activity, inhibits endocytic trafficking of cargo, and causes delay in EGFR degradation (30). Here, we confirmed that DRG2 depletion prolongs EGFR localization in Rab5-containing endosomes. In control cells, most EGFRs were absent from Rab5-containing endosomes at 30 min after EGF treatment; in DRG2-depleted cells, a large portion of EGFRs remained associated with

Rab5 endosomes until 180 min after EGF treatment (Supplementary Fig. S2). Endosomal insulin receptor has been shown to increase Akt phosphorylation and reduce GSK3 activity (26). Given that signaling occurs from EGFRs in both the plasma membrane and in endosomes (43), we wondered whether endosomal EGFRs enhance Akt activity and GSK3β phosphorylation. To test this, control and DRG2-depleted cells were starved and stimulated with 100 ng/ml of EGF, an inducer of Akt activity. We then analyzed the level of phosphorylated Akt in a time course experiment. Stimulation of serum-starved cells with EGF induced Akt phosphorylation to a greater extent and for a longer duration in DRG2-depleted cells than in control cells (Fig. 4A). We next visualized active Akt in living cells using FRET microscopy. In control cells, distinct FRET signals for active Akt were detected at 5 min following EGF stimulation, increased until 30 min, then decreased to background levels at 180 min (Fig. 4B). In DRG2-depleted cells, FRET signals for active Akt were detected in the absence of EGF stimulation and further increased to higher levels than in control cells at 5 min and 30 min following EGF stimulation. At 180 min after EGF stimulation, FRET signals in DRG2-depleted cells decreased but remained higher than in control cells (Figure 4B). Interestingly, most active Akt signals in DRG2-depleted cells were found in the cytoplasm and nucleus and not on the cell surface. Consistently, when Akt phosphorylation was monitored using antibodies, that following EGF stimulation in DRG2-depleted cells was greater and more sustained than in control cells (Fig. 4C). In addition, most phosphorylated Akt in DRG2-depleted cells was in cytoplasmic endosome-like structures. These results suggest that DRG2 depletion enhances Akt activity, and that most active Akt in the DRG2-depleted cells localizes to cytoplasmic endosome structures rather than on the cell surface.

We next analyzed levels of phosphorylated GSK3β in control and DRG2-depleted cells.

In DRG2-depleted cells, the level of phosphorylated GSK3β at Ser-9 was greater than in control cells and remained high until 180 min after EGF stimulation (Fig. 4A). Total GSK3β level was unchanged by EGF treatment. These results suggest that DRG2 depletion enhances inhibitory phosphorylation of GSK3β. To determine whether PI3K/Akt signaling mediates the inhibitory phosphorylation of GSK3β, we measured the level of phospho-GSK3β in DRG2-depleted cells in the presence of PI3K inhibitor LY294002 (Fig. 4D). LY294002 treatment reduced phosphorylation of both Akt and GSK3β in DRG2-depleted cells.

To determine whether inhibition of GSK3β is responsible for hyper-stabilization of microtubules and Golgi fragmentation, control HeLa cells were treated with LiCl, an inhibitor of GSK3β, and analyzed for acetylated tubulin level and Golgi structure. LiCl increased the inhibitory phosphorylation of GSK3β and microtubule acetylation (Fig. 4E) and induced Golgi fragmentation (Fig. 4F). Collectively, these results suggest that DRG2 depletion increases inhibitory phosphorylation of GSK3β by enhancing Akt activity, causing hyper-stabilization of microtubules and Golgi fragmentation.

**Inhibition of endocytosis reduces Akt activity and GSK3β phosphorylation and restores Golgi stacking in DRG2-depleted cells**

To determine whether EGFR signaling in endosomes causes the observed increase in Akt activity and GSK3β phosphorylation in DRG2-depleted cells, we inhibited EGFR endocytosis using a dominant-negative K44A dynamin mutant (44). DRG2-depleted cells were co-transfected with K44A dynamin and analyzed for phosphorylated Akt and GSK3β at 30 min following EGF treatment. Overexpression of K44A dynamin reduced Akt and GSK3β phosphorylation in DRG2-depleted cells (Fig. 5A). We also used the dynamin inhibitor dynasore to block endocytosis in DRG2-depleted cells. Consistently, dynasore treatment

reduced levels of phosphorylated Akt and GSK3β in DRG2-depleted cells at 30 min after EGF treatment (Fig. 5B). These results suggest that endosomal Akt signaling is responsible for the increase in Akt activity and inhibitory phosphorylation of GSK3β in DRG2-depleted cells.

We then investigated whether inhibition of endocytosis reduces microtubule stability and Golgi fragmentation. Dynasore treatment reduced tubulin acetylation (Fig. 5B) and restored Golgi stacks (Fig. 5C) in DRG2-depleted cells, indicating that hyper-stabilization of microtubules and Golgi fragmentation in DRG2-depleted cells depend on endocytosis.

**DRG2 depletion reduces Tau phosphorylation and increases colocalization of Tau with microtubules**

Tau is an important microtubule-associated protein which stabilizes microtubules in both neuronal[17] and non-neuronal cells (18). GSK3β suppresses microtubule stability through phosphorylation of Tau, which causes Tau to dissociate from the slightly acidic microtubule surface (20). This prompted us to test whether the increased phosphorylation of GSK3β in DRG2-depleted HeLa cells affects phosphorylation of Tau. Lysates of control and DRG2-depleted cells collected 30 min after EGF treatment were immunoblotted with anti-Tau antibodies. DRG2 depletion did not affect overall expression of Tau in Hela cells (Fig. 5D). However, the level of phosphorylated Tau at the threonine p231 epitope in DRG2-depleted cells was significantly lower than in control cells (Fig. 5D). Inhibition of endocytosis by dynasore increased Tau phosphorylation without affecting the total Tau level in DRG2-depleted cells (Fig. 5E). Tau has been reported to display both nuclear (45) and cytoplasmic localization in HeLa cells (46). We next determined the effect of DRG2 depletion on Tau localization. Control and DRG2-depleted cells were transfected with EGFP-α-tubulin. At 30

min after EGF treatment, cells were fixed and stained with anti-Tau antibody. Tau showed much greater colocalization with α-tubulin in DRG2-depleted cells than in control cells (Fig. 5F). These data suggest that DRG2 depletion increases microtubule stability by reducing Tau phosphorylation and enhancing association of Tau with microtubules.

**DRG2 depletion inhibits Golgi repositioning and cell migration**

The Golgi apparatus is a key regulator of directional cell movement. In wound healing assays, the Golgi and MTOC are repositioned to orient in the direction of migration (47). Golgi fragmentation inhibits cell migration (48). We thus sought to determine whether DRG2-depleted cells with fragmented Golgi showed defects in migration. In a wound healing assay, control cells moved into the wound area to fill the gap within 48 h, while DRG2-depleted cells failed to close the gap in this time period (Fig. 5G). Control cells treated with GSK3β inhibitor LiCl showed reduced migration (Figs. 5G), indicating that cell migration is affected by GSK3β activity. Consistently, while the Golgi of control cells polarized directionally towards the wound, DRG2-depleted cells did not show Golgi polarization toward the wound (Fig. 5H). To analyze the effect of DRG2 depletion on the repositioning of Golgi during cell migration, control and DRG2-depleted cells were co-transfected with fluorophore-tagged α-tubulin and Golgi marker, Golgi-7. Fluorescence traces of α-tubulin and Golgi-7 within cells showed that, in control cells, perinuclear MTOC and Golgi structures were evident and were repositioned to orient in the direction of migration (Fig. 5I and Supplementary Movie 3A). However, DRG2-depleted cells did not have perinuclear MTOC and Golgi structures and showed defects in repositioning of these structures and in cell migration (Fig. 5I and Supplementary Movie 3B). These results suggest that DRG2 depletion blocks repositioning of Golgi in the direction of migration and inhibits cell migration.

## Figure Legends

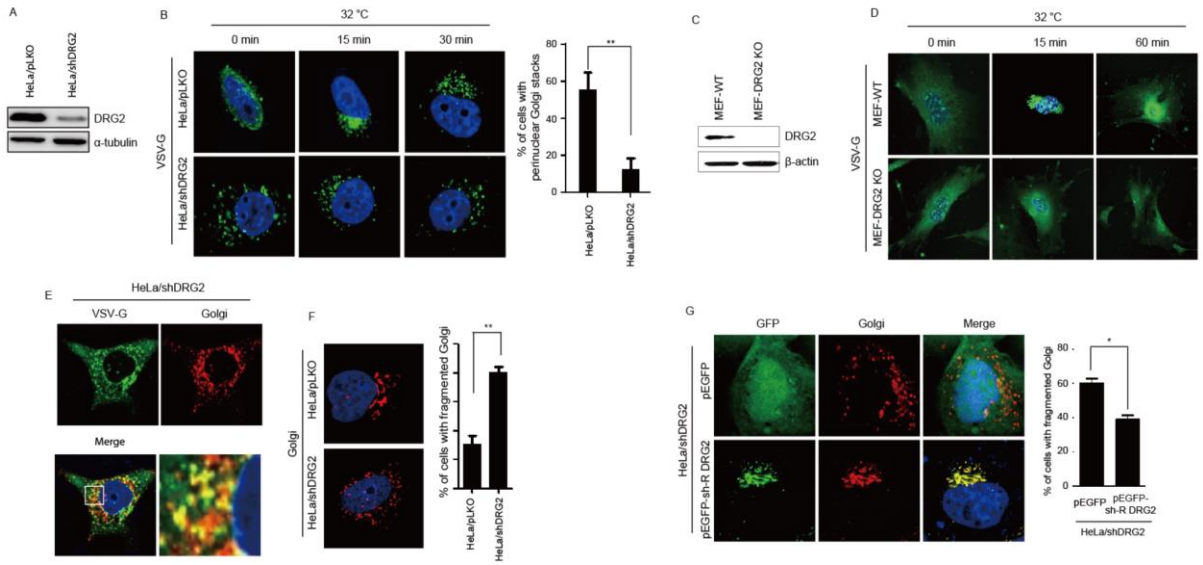


**Figure 1**. **DRG2 depletion induces Golgi fragmentation.** (A-E) VSV-G does not concentrate at perinuclear regions in DRG2-depleted cells. Western blot analysis of the DRG2 expression in HeLa/pLKO and HeLa/shDRG2 cells (A), and in MEF-WT and MEF-DRG2 KO cells (C). Control and DRG2-depleted HeLa cells (B) and MEF-WT and MEF-DRG2 KO cells (D) were transfected with VSV-G ts 045-GFP and incubated at 40.5℃ for 16 h. After further incubation with 100 μM cycloheximide for 30 min, cells were shifted to 32℃, incubated for indicated time period (chase). Nuclei were stained with DAPI (blue). Representative confocal microscopic images of cells. Graph in (B) indicates the percentage of cells with perinuclear Golgi at 15 min after shifting to 32℃. (E) Control and DRG2-depleted HeLa cells were cotransfected with VSV-G ts 045-GFP and tdTomato-Golgi-7 and incubated at 40.5℃ for 16 h. After further incubation with 100 μM cycloheximide for 1 hour, cells were shifted to 32℃ and incubated for 15 min. Representative confocal microscopic images of cells. Graph in (B) indicates the percentage of cells with perinuclear Golgi stacks at 15 min after shift to 32℃. Twenty cells were counted for each sample in triplicates. $^{**}p<0.01$. (F) DRG2 depletion results in a fragmented Golgi phenotype. HeLa/pLKO and HeLa/shDRG2

cells were stained with anti-GM130 antibody Nuclei were stained with DAPI (blue). Representative confocal images are shown. Graph indicates the percentage of cells with fragmented Golgi. Twenty cells were counted for each sample in triplicates. $^{**}p<0.01$. (G) Ectopic expression of DRG2 rescues Golgi structure in DRG2-depleted cells. DRG2-depleted HeLa cells were cotransfected for 24 h with the siRNA-resistant DRG2 and tdTomato-Golgi-7 constructs. Nuclei were stained with DAPI (blue). Representative confocal images are shown. Graph indicates the percentage of cells with fragmented Golgi. Twenty cells were counted for each sample in triplicates. $^{*}p<0.05$.

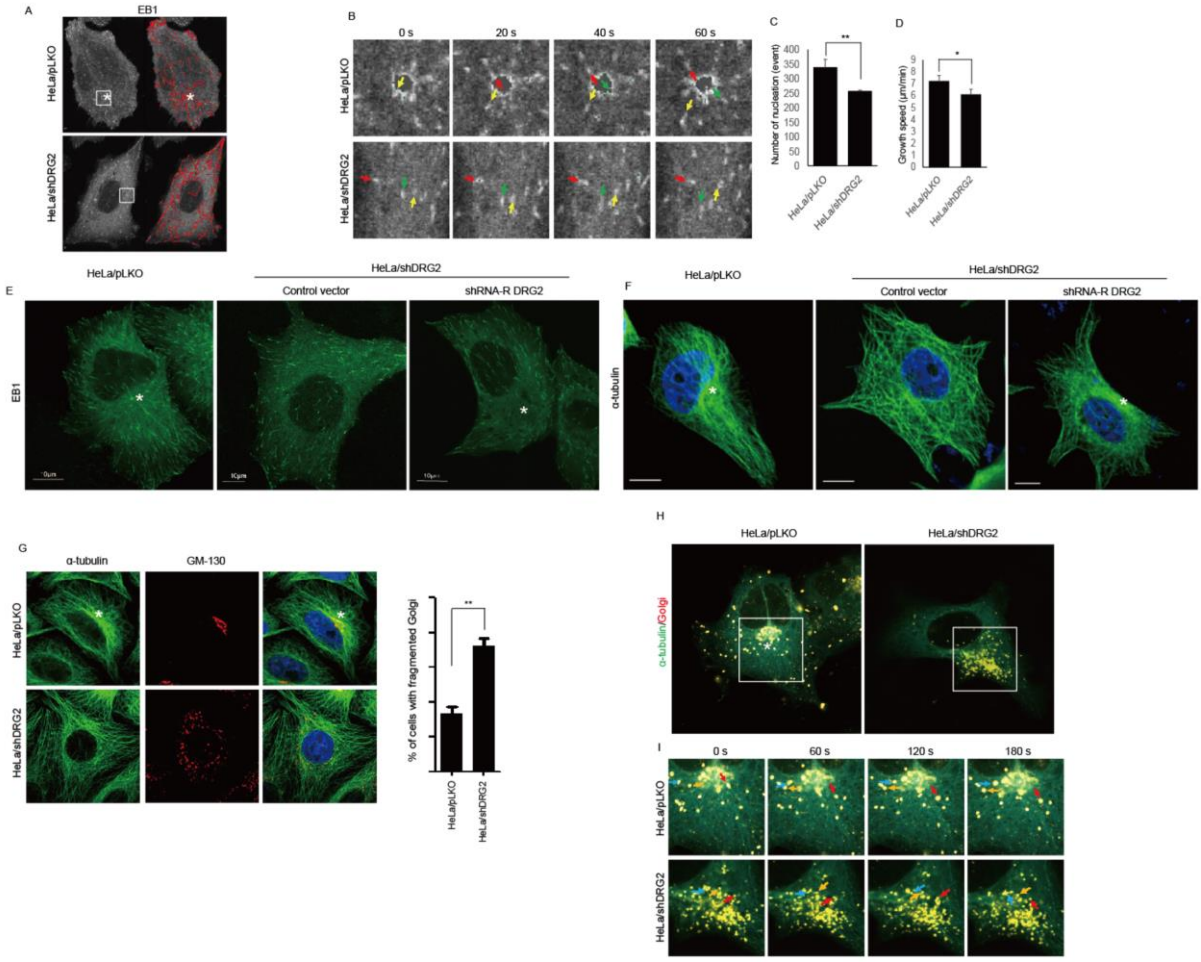


**Figure 2. Perinuclear MTOC formation and microtubule dynamics are inhibited in DRG2-depleted cells.** (A-D) DRG2 depletion inhibits microtubule nucleation from the perinuclear MTOC and microtubule growth. Control and DRG2-depleted HeLa cells were transfected with EB1-GFP to mark the plus end of growing microtubules. (A) Representative confocal images of control and DRG2-depleted Hela cells expressing EB1-GFP. The asterisk (*) marks the position from which the growing plus ends originate. EB1-EGFP comet tracks were recorded using plusTipTracker software. (B) Time series of EB1-GFP comets in the boxed region of (A). Each colored arrow follows a single EB1-GFP comet. Arrows indicate direction of EB1 migration (Suppl. Material Movies 1A, 1B). Time is indicated in seconds. Microtubule nucleation events (C) and speed of GFP-EB1 puncta (D) were measured in control and DRG2-depleted Hela cells. n=20 from three independent experiments. Data are

mean±SD; *$p$ <0.05, **$p$<0.01. (E, F) Ectopic expression of DRG2 rescues formation of perinuclear MTOC in DRG2-depleted cells. (E) DRG2-depleted HeLa cells were co-transfected with EB1-GFP and control vector or shRNA-resistant DRG2 constructs. Representative confocal images are shown. (F) DRG2-depleted HeLa cells were transfected with control vector or shRNA-resistant DRG2 constructs. Cells were fixed and stained with anti-α-tubulin antibody. Nuclei were stained with DAPI (blue). The asterisk (*) marks the MTOC. (G and H) Golgi-derived vesicles did not concentrate at perinuclear MTOC in DRG2-depleted cells. Control and DRG2-depleted HeLa cells were (G) stained with anti-α-tubulin and anti-GM130 antibodies or (H) co-transfected with EGFP-α-tubulin-GFP and tdTomato-Golgi-7. The asterisk (*) marks the MTOC. (I) Time series of Golgi vesicles migration in the boxed region of (H). Each colored arrow follows a single Golgi vesicle. Arrows indicate direction of Golgi vesicle migration (Suppl. Material Movies 2A, 2B).

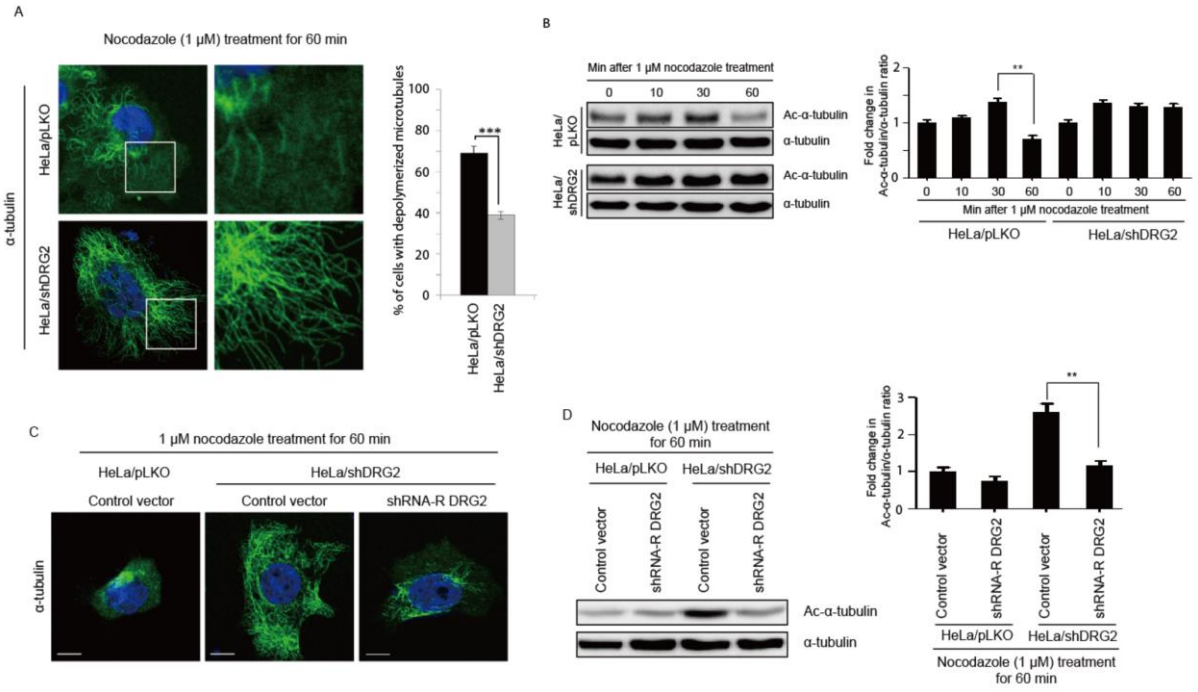


**Figure 3**. **DRG2 depletion enhances microtubule stability.** (A, B) DRG2 depletion confers resistance to the microtubule disrupting agent nocodazole. Control and DRG2-depleted HeLa cells were treated with 1 μM nocodazole for the indicated times. (A) Microtubules were visualized by immunofluorescent staining with anti-α- tubulin antibody. Nuclei were stained with DAPI (blue). Representative confocal images of microtubules are shown. The boxed regions were viewed at higher magnification. The graph indicates percentage of cells with depolymerized microtubules. Twenty cells were counted for each sample in triplicate. ***$p$<0.001. (B) Amounts of acetylated and total α-tubulin in cells treated with nocodazole were determined by immunoblotting with anti-acetylated α-tubulin and anti-α-tubulin antibodies. Graphs shows mean±SD (n=3) fold change in acetylated α-tubulin/total α-tubulin ratio with levels in cell 0 min after nocodazole treatment set to 1. **$p$<0.01. (C, D) Ectopic expression of DRG2 reduces resistance to nocodazole in DRG2-depleted cells. DRG2-depleted HeLa cells were transfected with control vector or shRNA-resistant DRG2 constructs. (C) Representative confocal images of cells stained with anti-α-tubulin antibodies.

Nuclei were stained with DAPI (blue). (D) The amounts of acetylated and total α- tubulin in the cells treated with nocodazole were determined by immunoblotting with anti-acetylated α-tubulin and anti-α-tubulin antibodies. Graphs shows mean±SD (n=3) fold change in acetylated α-tubulin/total α-tubulin ratio with levels in HeLa/pLKO transfected with control vector set to 1. $^{**}p<0.01$.

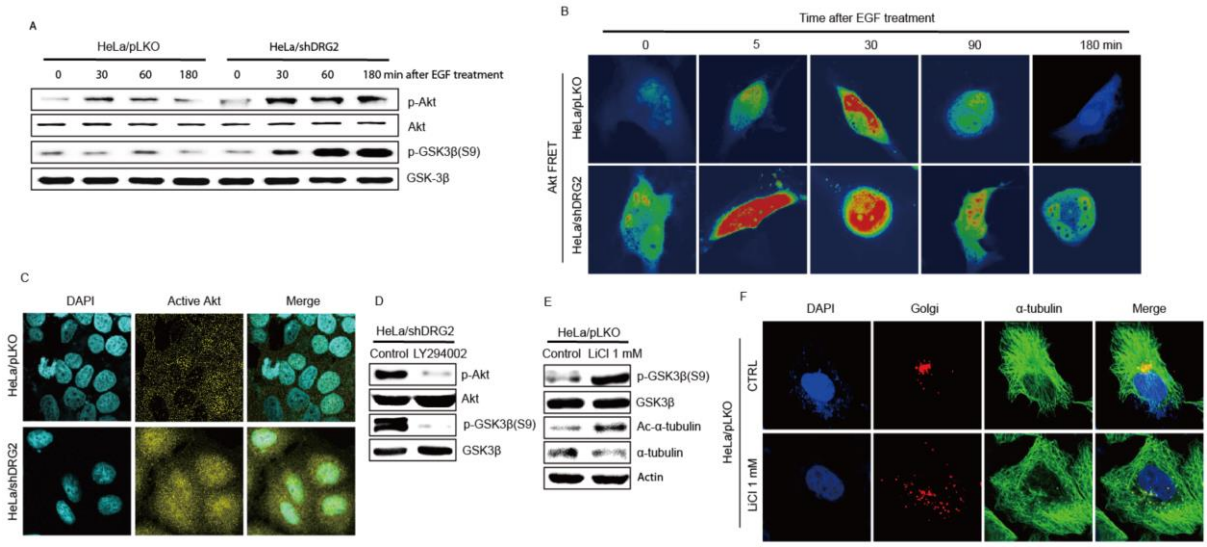


**Figure 4**. **DRG2 depletion increases Akt activity and inhibitory phosphorylation of GSK3β.** (A) Time course measurement of Akt and GSK3β phosphorylation in control and DRG2-depleted HeLa cells after EGF treatment. Cells were serum starved for 12 h and then stimulated with 100 ng/mL EGF for the times indicated. Cell lysates were analyzed for total and phosphorylated Akt and GSK3β by Western blot. (B) FRET analysis of Akt activity. (C) Immunohistochemical staining for active Akt. (D) PI3K inhibitor reduces phosphorylation of Akt and GSK3β in DRG2-depleted cells. DRG2-depleted HeLa cells were treated with 50 μM LY294002. Cell lysates were analyzed for total and phosphorylated Akt and GSK3β by Western blot. (E, F) Inhibition of GSK3β by LiCl phenocopies the effect of DRG2 depletion on microtubule stability and Golgi fragmentation. Control HeLa cells were transfected with tdTomato-Golgi-7 and treated with 1 mM LiCl. (E) Expression levels of phosphorylated GSK3β, total GSK3β, total tubulin and acetylated tubulin. (F) Cells were fixed and stained with anti-α-tubulin antibody. Representative confocal microscopic images of microtubules and Golgi structures are shown. Nuclei were stained with DAPI (blue).

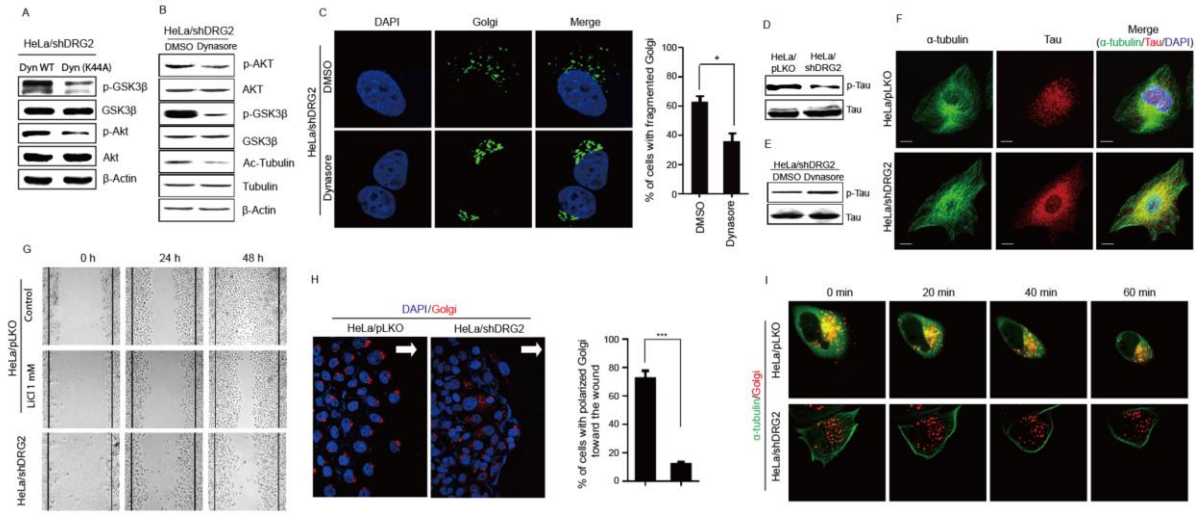


**Figure 5. Inhibition of endocytosis reduces phosphorylation of Akt and GSK3β and rescues Golgi stacks in DRG2-depleted cells.** (A) Expression of the dominant negative dynamin mutant Dyn K44A inhibits phosphorylation of Akt and the inhibitory phosphorylation of GSK3β in DRG2-depleted cells. DRG2-depleted HeLa cells were transfected with wild-type or dominant negative dynamin mutant K44A. After 12 h of serum starvation, cells were treated with 100 ng/mL EGF for 1 h. Cells were analyzed for phosphorylated Akt and GSK3β and acetylated tubulin by Western blot. (B) Dynamin inhibitor inhibits phosphorylation of Akt and GSK3β in DRG2-depleted cells. DRG2-depleted HeLa cells were transfected with EGFP-EGFR. After 12 h of serum starvation, cells were treated with 80 μM dynasore for 30 min and further incubated with 100 ng/mL EGF for 1 h. Cells were analyzed for phosphorylated Akt and GSK3β and acetylated tubulin by Western blot. (C) Dynasore treatment rescues Golgi stacks in DRG2-depleted cells. DRG2-depleted cells were transfected with mEmerald Golgi-7, treated with 80 μM dynasore for 30 min and further incubated with 100 ng/mL EGF for 1 h. Nuclei were stained with DAPI (blue). Representative confocal images are shown. (D) DRG2 depletion reduces Tau phosphorylation and increases co-localization of Tau with microtubules. Control and DRG2-depleted HeLa cells were serum starved for 12 h and incubated with 100 ng/mL EGF for 1 h.

Cell lysates were analyzed for the levels of total and pT231 Tau by Western blot. (E) Dynasore treatment restores Tau phosphorylation in DRG2-depleted cells. DRG2-depleted cells were treated with 80 μM mM dynasore for 30 min and further incubated with EGF 100 ng/mL for 1 h. Cell lysates were analyzed for the levels of total and pT231 Tau by Western blot. (F) DRG2 depletion increases co-localization of Tau with microtubules. Control and DRG2-depleted HeLa cells were transfected with EGFP-α-tubulin and incubated with 100 ng/mL EGF for 1 h. Cells were stained with anti-Tau antibody. Representative images from three experiments. (G) DRG2 depletion inhibits cell migration. Wound healing assays were performed using control and DRG2-depleted HeLa cells in the absence or presence of the GSK3β inhibitor LiCl (1 mM). Representative images from three experiments. The graph represents quantification of restored surface from three experiments. Data are mean ± SD ($n$ = 3) (**$p$ < 0.01). (H) DRG2 depletion inhibits directional polarization of Golgi. Wound healing assays were performed using control and DRG2-depleted HeLa cells. After incubation for 24 h, cells were stained with DAPI (blue) and with anti-GM130 antibody (red). Representative confocal images are shown. Arrows indicate direction toward the wound. Graph indicates the percentage of cells with Golgi polarization toward the wound. Twenty cells were counted for each sample in triplicates. ***$p$<0.001. (I) Control and DRG2-depleted HeLa cells were co-transfected with EGFP-a-tubulin and tdTomato-Golgi-7. Frames from representative movies of migrating cells in the wounded area are shown. Scale bars: 10 μm. Movies of the cells shown are in Suppl. Materials Movies 3A and 3B.

**Discussion**

In this study, we demonstrated that DRG2 depletion enhances Akt activity and inhibitory phosphorylation of GSK3β, which leads to hypo-phosphorylation of Tau, hyper-stabilization of microtubules, and disappearance of perinuclear MTOC. DRG2 depletion induced Golgi fragmentation and inhibits accumulation of VSV-G in perinuclear Golgi stacks. In addition, DRG2-depleted cells showed defects in repositioning of Golgi stacks toward the leading edge, which is required for cell migration (49). These findings reveal a new role of DRG2 in Golgi fragmentation and cell migration.

The perinuclear stacking of Golgi depends on the microtubule network and perinuclear MTOC (5, 6). Golgi-derived vesicles and Golgi mini-stacks move along microtubules toward the MTOC and are concentrated in the perinuclear region (38). DRG2 depletion inhibited formation of perinuclear MTOC formation and induced Golgi fragmentation. Microtubule depolymerization by nocodazole leads to disappearance of perinuclear MTOC, Golgi fragmentation (12, 50), and prevents accumulation of VSV-G in perinuclear Golgi stacks (37). Since DRG2 depletion inhibited MTOC formation, perinuclear Golgi stacking, and accumulation of VSV-G in perinuclear Golgi stacks, we expected that DRG2 depletion would reduce microtubule stability. However, we found that DRG2 depletion increased microtubule stability. Hyperstabilization of microtubules by taxol leads to disappearance of perinuclear MTOC and Golgi fragmentation (16). Consistent with this observation, we found that microtubules in DRG2-depleted cells were more resistant to nocodazole-induced depolymerization. Furthermore, microtubule growth (measured by analyzing EB1 comets) was significantly inhibited in DRG2-depleted cells. These results suggest that DRG2 depletion enhances microtubule stability, which inhibits perinuclear MTOC and Golgi stack formation.

Tau is a microtubule-associated protein which is essential for microtubule assembly (51). GSK3β phosphorylates Tau, reducing microtubule stability (41). GSK3β is a constitutively active kinase, and phosphorylation at Ser-9 inhibits its activity (42). We found that DRG2 depletion increased the inhibitory phosphorylation at Ser-9 of GSK3β. Consistently, we found that DRG2 depletion reduced Tau phosphorylation and enhanced Tau-microtubule association. We also found that treatment of cells with the GSK3β inhibitor LiCl increased microtubule stability, induced Golgi fragmentation, and inhibited cell migration. These results indicate that DRG2 depletion inhibits GSK3β activity and Tau phosphorylation, resulting in enhanced microtubule stability.

How does DRG2 depletion increase GSK3β phosphorylation? GSK3β Ser-9 phosphorylation is mediated by the PI3K/Akt signaling pathway (42). We found that Akt activity following EGF treatment is greater in DRG2-depleted cells than in control cells. PI3K inhibitor reduced phosphorylation of Akt and GSK3β at Ser-9. Thus, Akt activity in DRG2-depleted cells is responsible for the increased GSK3β Ser-9 phosphorylation. Upon stimulation with EGF, EGFR can activate downstream signaling pathways in either the plasma membrane or in endosomes (43). We previously reported that DRG2-depleted cells contain high levels of endosomal EGFR due to defects in EGFR degradation (30). This suggests the possibility that DRG2-depleted cells have enhanced signaling from endosomal EGFRs, which activates Akt. In this study, we provide evidence to support this hypothesis. Most of the active Akt in DRG2-depleted cells was detected within the cells and not on the membrane surface; furthermore, inhibition of endocytosis by either a dominant-negative mutant dynamin (44) or by the dynamin inhibitor dynasore reduced Akt activity and GSK3β Ser9 phosphorylation, increased Tau phosphorylation, reduced tubulin acetylation, and rescued the formation of Golgi stacks in DRG2-depleted cells.

Overall, our data indicate that DRG2 depletion upregulates Akt signaling, resulting in inhibitory phosphorylation of GSK3β that reduces Tau phosphorylation. Consequently, microtubules are hyper-stabilized, and perinuclear MTOC formation is inhibited, leading to Golgi fragmentation. Golgi fragmentation causes loss of directional cell migration (Supplementary Fig. S3). Therefore, our results suggest that DRG2 is a key regulator of the Akt/GSK3β signaling pathway and of microtubule stability and Golgi structure in cells. Given that microtubule structural defects and Golgi fragmentation have been observed in neurodegeneration and other diseases, our findings may improve the understanding of pathogenesis of these diseases and identifies DRG2 as a potential therapeutic target.

## Reference


1. Rambourg, A., Clermont, Y., Hermo, L., and Segretain, D. (1987) Tridimensional structure of the Golgi apparatus of nonciliated epithelial cells of the ductuli efferentes in rat: an electron microscope stereoscopic study. *Biol. Cell* **60**, 103–115
2. Ladinsky, M. S., Mastronarde, D. N., McIntosh, J. R., Howell, K. E, and Staehelin, L. A. (1999) Golgi structure in three dimensions: functional insights from the normal rat kidney cell. *J. Cell Biol*. **144**, 1135–1149
3. Hu, Z., Zeng, L., Huang, Z., Zhang, J., and Li, T. (2007) The study of Golgi apparatus in Alzheimer's disease. *Neurochem. Res.* **32**, 1265–1277
4. Ungar, D. (2009) Golgi linked protein glycosylation and associated diseases. *Semin Cell Dev. Biol.* **20**, 762–769
5. Glick, B. S., and Nakano, A. (2009) Membrane traffic within the Golgi apparatus. *Annu. Rev. Cell Dev. Biol.* **25**, 113–132
6. Yadav, S., and Linstedt, A. D. (2001) Golgi positioning. *Cold Spring Harb. Perspect. Biol.* **3**, a005322
7. Cardenas, J., Rivero, S., Goud, B., Bornens, M., and and Rios, R. M. (2009) Golgi localization of GMAP210 requires two distinct cis-membrane binding mechanisms. *BMC Biol.* **56**.
8. Rios, R. M., and Bornens, M. (2003) The Golgi apparatus at the cell centre. *Curr. Opin. Cell Biol.* **15**, 60–66
9. Rios, R. M., Sanchís, A., Tassin, A. M., Fedriani, C., and Bornens, M. (2004) GMAP-210 recruits gamma-tubulin complexes to cis-Golgi membranes and is required for Golgi ribbon formation. *Cell* **118**, 323–335
10. Miller, P. M., Folkmann, A. W., Maia, A. R., Efimova, N., Efimov, A., and Kaverina, I. (2009) Golgi-derived CLASP-dependent microtubules control Golgi organization and polarized trafficking in motile cells. *Nat. Cell Biol.* **11**, 1069–1080

11. *Mitchison, T., and Kirschner, M. (1984) Dynamic instability of microtubule growth. Nature **312**, 237–242*
12. Thyberg, J., and Moskalewski, S. (1958) Microtubules and the organization of the Golgi complex. *Exp. Cell Res.* **159**, 1–16
13. Ho, W. C., Allan, V. J., Van Meer, G., Berger, E. G., and Kreis, T. E. (1989) Reclustering of scattered Golgi elements occurs along microtubules. *Eur. J. Cell Biol.* **48**, 250–263
14. DeBrabander, M., Gevens, G., Nuydens, R., Willebrords, R., and De Mey, J. (1981) Taxol induces the assembly of free microtubules in living cells and blocks the organizing capacity of the centrosomes and kinetochores. *Proc. Natl. Acad. Sci. USA* **78**, 5608-5612
15. Schiff, P. B., and Horwitz, S. B. (1980) Taxol stabilizes microtubules in mouse fibroblast cells. *Proc. Natl. Acad. Sci. USA* **77**, 1561–1565
16. Wehland, J., Henkart, M., Klausner, R., and Sandoval, I. V. (1980) Role of microtubules in the distribution of the Golgi apparatus: Effect of taxol and microinjected anti-α-tubulin antibodies. *Proc. Natl. Acad. Sci. USA* **80**, 4286-4290
17. Drechsel, D. N., Hyman, A. A., Cobb, M. H. and Kirschner, M. W. (1992) Modulation of the dynamic instability of tubulin assembly by the microtubule-associated protein tau. *Mol. Biol. Cell* **3**, 1141-1154
18. Lee, G., and Rook, S. L. (1992) Expression of tau protein in non-neuronal cells: microtubule binding and stabilization. *J. Cell Sci.* **10**, 227-237
19. Hernández, F., and Avila, J. (2007) Tauopathies. *Cell Mol. Life Sci*. **64**, 2219-2233
20. Lovestone, S. Reynolds, C. H., Latimer, D., Davis, D. R., Anderton, B. H., Gallo, J. M., Hanger, D., Mulot, S., Marquardt, B., Stabel, S., Woodgett, J. R., and Miller C. J. (1994) Alzheimer's disease-like phosphorylation of the microtubule-associated protein tau by glycogen synthase kinase-3 in transfected mammalian cells. *Curr. Biol.* **4**, 1077-1086
21. Murphy, J. E., Padilla, B. E., Hasdemir, B., Cottrell, G. S., and Bunnett, N. W. (2009) Endosomes: A legitimate platform for the signaling train. *Proc. Natl. Acad. Sci. USA* **106**, 17615–17622

22. Miaczynska, M., Christoforidis, S., Giner, A., Shevchenko, A., Uttenweiler-Joseph, S., Habermann, B., Wilm, M., Parton, R. G., and Zerial, M. (2004) APPL proteins link Rab5 to nuclear signal transduction via an endosomal compartment. *Cell* **116**, 445–456

23. Lin, D. C., Quevedo, C., Brewer, N. E., Bell, A., Testa, J. R., Grimes, M. L., Miller, F. D., and Kaplan, D. R. (2006) APPL1 associates with TrkA and GIPC1 and is required for nerve growth factor-mediated signal transduction. *Mol. Cell Biol.* **26**, 8928–8941

24. Schenck, A., Goto-Silva, L., Collinet, C., Rhinn, M., Giner, A., Habermann, B., Brand, M., and Zerial, M. (2008) The endosomal protein Appl1 mediates Akt substrate specificity and cell survival in vertebrate development. *Cell* **133**, 486–497

25. Hunker, C. M., Kruk, I., Hall, J. Giambini, H., Veisaga, M. L., and Barbieri, M. A. (2006) Role of Rab5 in insulin receptor-mediated endocytosis and signaling. *Arch. Biochem. Biophys.* **449**, 130-142

26. Braccini, L., Ciraolo, E., Campa, C. C. Perino, A., Longo, D. L., Tibolla, G., Pregnolato, M., Cao, Y., Tassone, B., Damilano, F., Laffargue, M., Calautti, E., Falasca, M., Norata, G. D., Backer, J. M., and Hirsch, E. (2015) PI3K-C2γ is a Rab5 effector selectively controlling endosomal Akt2 activation downstream of insulin signaling. *Nat. Commun.* **6**, 7400

27. Su, X., Lodhi, I.. J., Saltiel, A. R., and Stahl, P. D. (2006) Insulin-stimulated Interaction between insulin receptor substrate 1 and p85alpha and activation of protein kinase B/Akt require Rab5. *J Biol Chem* **281**, 27982–27990

28. Schenker, T., Lach, C., Kessler, B., Calderara, S., and Trueb, B. (1994) A Novel Gtp-Binding Protein Which Is Selectively Repressed in Sv40-Transformed Fibroblasts. *J. Biol. Chem.* **269**, 25447-25453

29. Li, B., and Trueb, B. (2000) DRG represents a family of two closely related GTP-binding proteins. *Biochim. Biophys. Acta.* **1491**, 196-204

30. Mani, M., Lee, U. H., Yoon, N. A., Kim, H. J., Ko, M. S., Seol, W., Joe, Y., Chung, H. T., Lee, B. J., Moon, C. H., Cho, W. J., and Park, J. W. (2016) Developmentally regulated GTP-

binding protein 2 coordinates Rab5 activity and transferrin recycling. *Mol. Biol. Cell* **27**, 334-348

31. Jang, S. H., Kim, A. R., Park, N. H., Park, J. W., and Han, I. S. (2016) DRG2 regulates G2/M progression via the cyclin B1-Cdk1 complex. *Mol. Cells* **39**, 699-704
32. Bolte, S., and Cordelieres, F. P. (2006) A guided tour into subcellular colocalization analysis in light microscopy. *J. Microsc.* **224**, 213–232
33. Applegate, K. T., Besson, S., Matov, A., Bagonis, M. H., Jaqaman, K., and Danuser, G. (2011) plusTipTracker: Quantitative image analysis software for the measurement of microtubule dynamics. *J. Struct. Biol.* **176**, 168–184
34. Gao, X., and Zhang, J. (2008) Spatiotemporal analysis of differential Akt regulation in plasma membrane microdomains. *Mol. Biol. Cell* **19**, 4366-4373
35. Zhou, X., Clister, T. L., Lowry, P. R., Seldin, M. M,, Wong, G. W., and Zhang, J. (2015) Dynamic Visualization of mTORC1 Activity in Living Cells. *Cell Rep.* **10**, 1767-1777
36. Kreis, T. E., and Lodish, H. F. (1986) Oligomerization is essential for transport of vesicular stomatitis viral glycoprotein to the cell surface. *Cell* **46**, 929–937
37. Presley, J. F., Cole, N. B., Schroer, T. A., Hirschberg, K., Zaal, K. J., and Lippincott-Schwartz, J. (1997) ER-to-Golgi transport visualized in living cells. *Nature* **389**, 81–85
38. Allan, V. J., Thompson, H. M., and McNiven, M. A. (2002) Motoring around the Golgi. *Nat. Cell Biol.* **4**, E236-E242
39. Schaub, B. E., Berger, B., Berger, E. G., and Rohrer, J. (2006) Transition of galactosyltransferase 1 from trans-Golgi cisterna to the Tran-Golgi network is signal mediated. *Mol. Biol. Cell* **17**, 5153-5162
40. Hammond, J. W., Cai, D., and Verhey, K. J. (2008) Tubulin modifications and their cellular functions. *Curr. Opin. Cell Biol.* **20**, 71–76
41. Hanger, D. P., Hughes, K., Woodgett, J. R., Brion, J. P., and Anderton, B. H. (1992) Glycogen synthase kinase-3 induces Alzheimer's disease-like phosphorylation of tau:

generation of paired helical filament epitopes and neuronal localisation of the kinase. *Neurosci. Lett.* **147**, 58-62

42. Dajani, R., Fraser, E., Roe, S. M., Young, N., Good, V., Dale, T. C., and Pearl, L. H. (2001) Crystal structure of glycogen synthase kinase 3 beta: structural basis for phosphate-primed substrate specificity and autoinhibition. *Cell* **105**, 721–732
43. Sorkin, A., and von Zastrow, M. (2009) Endocytosis and signalling: intertwining molecular networks. *Nat Rev Mol. Cell Biol.* **10**, 609-622
44. Vieira, A. V., Lamaze, C., and Schmid, S. L. (1996) Control of EGF receptor signaling by clathrin-mediated endocytosis. *Science* **274**, 2086-2089
45. Sjöberg, M. K., Shestakova, E., Mansuroglu, Z., Maccioni, R. B, and Bonnefoy, E. (2006) Tau protein binds to pericentromeric DNA: a putative role for nuclear tau in nucleolar organization. *J. Cell Sci.* **119**, 2025-2034
46. Mohamed, N. V., Desjardins, A., and Leclerc, N. (2017) Tau secretion is correlated to an increase of Golgi dynamics. *PLoS ONE* **12**, e0178288
47. Kupfer, A., Dennert, G., and Singer, S. J. (1983) Polarization of the Golgi apparatus and the microtubule-organizing center within cloned natural killer cells bound to their targets. *Proc. Natl. Acad. Sci. USA* **23**, 7224–7228
48. Yadav, S., Puri, S., and Linstedt, A. D. (2009) A Primary Role for Golgi Positioning in Directed Secretion, Cell Polarity, and Wound Healing. *Mol. Biol. Cell* **20**, 1728–1736
49. Chen, B., Kumar, G., Co, C. C., and Ho, C. C. (2013) Geometric control of cell migration. *Sci. Rep.* **3**, 2827
50. Cole, N. B., Sciaky, N., Marotta, A., Song, J., and Lippincott-Schwartz, J. (1996) Golgi dispersal during microtubule disruption: regeneration of Golgi stacks at peripheral endoplasmic reticulum exit sites. *Mol. Biol. Cell* **7**, 631-650
51. Weingarten, M. D., Lockwood, A. H., Hwo, S. Y., and Kirschner, M. W. (1975) A protein factor essential for microtubule assembly. *Proc. Natl. Acad. Sci. USA* **72**, 1858-1862

## 국문요약

미세소관의 유동성에 의해 유지되는 골지체의 핵 주변부 형성은 세포의 이동에 있어서 필수적이다. DRG2 는 미세소관의 안정성, 핵 주변부의 골지체 형성, 세포의 이동에 있어서 중요한 역할을 한다. DRG2 의 감소는 소포체 내부 EGFR 을 오래 머무르게 하고, 이는 AKT 활성과 GSK3β 의 억제형태 인산화를 강화시킨다. DRG2 가 감소된 세포에서 GSK3β 의 억제에 의해 Tau 는 낮은 수준의 인산화가 일어나고, 미세소관과 높은 결합을 보이고, 그에 따른 결과로 미세소관이 안정화된다. 안정화된 미세소관은 Nocodazole 에 의한 미세소관 분해에 저항성을 가지게 된다,. DRG2 가 감소된 세포에서는 미세소관의 성장과 미세소관 조직 센터(MTOC)의 형성, 골지체의 조각화 세포이동의 방향성이 손실되어 있다. 이러한 결과들은 핵 주변부의 골지체 형성, GSK3β 인산화가 세포의 이동에 미치는 영향과 미세소관 안정화를 조절하는 DRG2 의 밝혀지지 않았던 기능을 설명한다.

**중심단어**: DRG2, GSK3β, 미세소관 안정화, 골지체 조각화, 세포이동